

DOI: 10.1070/QEL16063

Propagation of femtosecond pulses in a hollow-core revolver fibre

Yu.P. Yatsenko, A.A. Krylov, A.D. Pryamikov, A.F. Kosolapov,
A.N. Kolyadin, A.V. Gladyshev, I.A. Bufetov

Abstract. **We have studied for the first time the propagation of femtosecond pulses through an optical fibre with an air-filled hollow core and a cladding in the form of one ring of noncontacting cylindrical capillaries for high-power radiation transmission in the 1.55-μm telecom range. Numerical analysis results demonstrate that the parameters of the fibre enable radiation transmission in the form of megawatt-power Raman solitons through up to a 25-m length of the fibre and tuning of the emission wavelength over 130 nm. We have experimentally demonstrated femtosecond pulse transmission through fibres up to 5 m in length in the linear propagation regime, without distortions of the pulse spectrum, with a dispersion-induced temporal pulse broadening within 20%.**

Keywords: *hollow-core fibres, femtosecond pulses, Raman solitons.*

1. Introduction

Hollow-core microstructured fibres offer unique possibilities for transmitting high-power femtosecond pulses over considerable distances owing to the high degree of localisation of their fundamental mode in their core. In optical fibres with a negative curvature of their core–cladding interface, the degree of localisation reaches 99.993% [1]. The main nonlinear medium that influences the shape and spectrum of femtosecond pulses is the gas filling the fibre core. Hollow-core microstructured fibres can ensure light–gas interaction lengths at which the nonlinear properties of the gas have a strong effect on the spectral and temporal characteristics of femtosecond pulses [2–7].

Optical fibres whose hollow core is filled with air at atmospheric pressure are of particular interest for producing all-fibre systems transmitting high-power femtosecond pulses, because they require no complex gas filling procedures. The propagation of high-power femtosecond pulses through a photonic crystal fibre having a hollow core filled with atmospheric air was studied by Ouzounov et al. [6]. The fibre had a transmission band from 1400 to 1550 nm and a dispersion parameter D = 15.9 ps nm^{-1} km^{-1}. When a 110-fs pulse of 900-nJ energy at a wavelength of 1470 nm was launched into a 3-m length of the fibre, the output pulse had a power of 2.4 MW and its spectrum was shifted towards the long-wavelength edge of the transmission band. Luan et al. [7] demonstrated transmission of pulses at 800-nm wavelength in an air-filled hollow-core photonic crystal fibre. Raman solitons at the output of a 5-m length of the fibre had 208-kW power and 290-fs duration. The dispersion parameter of the fibre at the above wavelength was 140 ps nm^{-1} km^{-1}.

The relatively short pulse propagation distances obtained in those studies are mainly due to the large Raman shift of the soliton spectrum towards the long-wavelength edge of the transmission band, where solitons are strongly absorbed. The Raman shift is directly related to the dispersion [8] and transmission bandwidth. In connection with this, there is special interest in high-power femtosecond pulse transmission through a hollow-core Kagome lattice photonic crystal fibre with a hypocycloid-shaped core–cladding interface [9, 10].

Wang et al. [9] described pulse transmission (1550 nm, 105 μJ, 844 fs) through a Kagome lattice fibre with a 70-μm-diameter air core. The fibre had a very broad transmission band, from 1100 to 1750 nm (with a loss of 40 ± 5 dB km^{-1}), and a dispersion D = 2 ps nm^{-1} km^{-1} in the range 1500–1600 nm. At the output of a 2.3-m length of the fibre, they obtained pulses with an energy of 78 μJ (power of 240 MW) and duration of 300 fs on account of soliton compression.

Debord et al. [10] reported a Kagome lattice fibre with a transmission band from 900 to 1300 nm and a loss of 200 dB km^{-1} at a wavelength of 1030 nm. The fibre had a high degree of localisation of its fundamental mode. The fraction of light propagating through the glass was at a level of 2.8 × 10^{-6}, with a mode field diameter of 64 μm. The calculated dispersion at a wavelength of 1030 nm was $\beta_2 = -0.45$ ps^2 km^{-1} (D = 0.8 ps nm^{-1} km^{-1}). When a 600-fs pulse of 800-μJ energy was launched into a 10-m length of the fibre, filled with ambient air, the output energy exceeded 350 μJ. In a 3-m length of an air-core fibre, the soliton regime was obtained, with a pulse energy above 100 μJ.

The type of fibre used by Wang et al. [9] and Debord et al. [10] can be assigned to a more general class: hollow-core microstructured fibres with a negative curvature of their core–cladding interface (the importance of a negative curvature of the interface for the guidance properties of the fibre was first pointed out by Pryamikov et al. [11]). This class also includes optical fibres with a cladding in the form of ice cream cones [12, 13] or a single ring of hollow capillaries [11], which were named 'revolver fibres' [14]. Compared to the hollow-core Kagome lattice fibres with a hypocycloid-shaped core boundary, the hollow-core revolver fibres (HCRFs) have a

Yu.P. Yatsenko, A.A. Krylov, A.D. Pryamikov, A.F. Kosolapov, A.N. Kolyadin, A.V. Gladyshev, I.A. Bufetov Fiber Optics Research Center, Russian Academy of Sciences, ul. Vavilova 38, 119333 Moscow, Russia; e-mail: yuriya@fo.gpi.ru, krylov@fo.gpi.ru

Received 4 March 2016; revision received 17 May 2016
Kvantovaya Elektronika **46** (7) 617–626 (2016)
Translated by O.M. Tsarev

simpler design, which allows for necessary monitoring of parameters in the fibre fabrication process. This offers the possibility of more accurately maintaining relationships between the effective mode area, dispersion and transmission bandwidth required for pulse delivery. Moreover, in the Kagome lattice fibres, two light localisation mechanisms coexist: a local mechanism, related to interaction between hollow-core modes with some limited parts of the core–cladding interface, and a nonlocal mechanism, related to interaction of light with the core boundary as a whole. In the latter case, resonance coupling between modes of the hollow core and core–cladding interface is possible, which is determined by the type of rotational symmetry of the shape of the core boundary [15] and makes it necessary to increase the hollow-core diameter in order to obtain a low total loss. An HCRF may have only one local mechanism of light localisation provided the cladding capillaries are separated by a distance comparable to the capillary radius. This type of HCRF was first proposed by Kolyadin et al. [16]. The possibility of obtaining analogous optical characteristics at smaller hollow-core diameters by placing cladding capillaries some distance apart is important for applications related to nonlinear effects that originate from the propagation of laser pulses in hollow-core fibres.

The propagation of femtosecond pulses in an HCRF at a wavelength of 0.748 μm was demonstrated by Kolyadin et al. [17]. A fibre with eight noncontacting capillaries and a core diameter of 21 μm had a transmission band from 700 to 800 nm. Pulses of 180-fs duration with an average input power of 1.3 W and repetition rate of 76 MHz were passed through a 10-m length of the fibre without distortion of their spectrum, with a twofold dispersion-induced temporal broadening, which corresponded to a measured dispersion of 7.7 ps nm^{-1} km^{-1}. The average output power was 100 mW.

In this paper, we examine the possibility of using an air-core HCRF for transmitting high-power femtosecond pulses in the 1.55-μm telecom range, important for practical application. To this end, the first HCRF with a broad transmission band in the 1.55-μm range has been fabricated. The propagation of high-power pulses through the fibre has been studied theoretically and experimentally in an insufficiently explored range of pulse durations (~100 fs), for which the spectral width is comparable to the transmission bandwidth of the fibre. Numerical analysis shows that, in the case of 100-fs pulses in the nonlinear regime, megawatt Raman solitons can propagate without broadening into a supercontinuum at fibre lengths of up to 25 m. Our experimental data confirm the propagation of femtosecond pulses of kilowatt power in the linear regime without spectral distortions over fibre lengths of up to 5 m.

2. Numerical experiment

The propagation of femtosecond erbium fibre laser (1560 nm) pulses through an HCRF was studied for powers limited from above by the critical power for self-focusing in air (~10 GW). Numerical simulation was performed for 100-fs transform-limited Gaussian pulses propagating in a fibre filled with atmospheric air at a pressure of 1 atm. The nonlinear and dispersion characteristics of atmospheric air have been rather well studied because the propagation of high-power optical pulses of various durations through the atmosphere has recently been the subject of intense research [18–25]. In particular, it has been shown that, at a pulse power below the critical power for self-focusing, the parameters of pulses propagating through air are influenced primarily by dispersion, Kerr nonlinearity and stimulated Raman scattering (SRS) by rotational transitions of nitrogen. The dispersion of air is low, $\beta_2 = 1.6 \times 10^{-1}$ fs^2 cm^{-1} [23], which allows Gaussian pulses with a full width at half maximum $\tau = 100$ fs to propagate in air without dispersion-induced broadening over a distance $L_d = t_0^2/\beta_2 = 225$ m ($t_0 = \tau/1.665$).

In the case of ~100-fs pulses, the Kerr effect and SRS make equal contributions to the nonlinear refractive index: $n_{2K} = n_{2R} = 3 \times 10^{-23}$ m^2 W^{-1} [19, 21–24]. The spectral width of 100-fs pulses (e^{-1} width of Gaussian pulses, 5.3 THz) is comparable to the 2.25 THz frequency (75 cm^{-1}) of the transition between the J = 8 and 6 levels of the N_2 molecule in the vibrational ground state. This results in highly time-dependent SRS conditions, under which the Raman gain coefficient and the dephasing time of the dipole moment of the excited rotational state are considerably smaller than those of steady-state SRS. In the case of ~100-fs pulses, the Raman gain coefficient in air is $g_R = 0.025$ cm TW^{-1} and the dipole relaxation time of the rotational transition in nitrogen is $\tau_{dip} = 76.9$ fs [22, 23].

In numerical analysis of the propagation of femtosecond pulses in a hollow-core fibre, we used a generalised nonlinear Schrödinger equation for the complex-valued spectral pulse envelope $\tilde{A}(z,\omega)$ in the form [26]

$$\frac{dA'}{dz} = i\bar{\gamma}(\omega)\exp[-i\hat{L}(\omega)z]$$

$$\times\Im\left\{\bar{A}(z,T)\int_{-\infty}^{\infty} R(T')\,|A(z,T-T')|^2 dT'\right\},$$

where the nonlinear response is given by

$$\bar{\gamma}(\omega) = \frac{n_2 n_0 \omega}{c n_{eff}(\omega) A_{eff}^{1/4}(\omega)}, \quad \bar{A}(z,T) = \Im^{-1}\left\{\frac{\tilde{A}(z,\omega)}{A_{eff}^{1/4}(\omega)}\right\}.$$

The variation of the variables is determined by $A'(z,\omega) = \tilde{A}(z,\omega)\exp[-\hat{L}(\omega)z]$, where the dispersion-controlling linear operator has the form

$$\hat{L}(\omega) = i\{\beta(\omega) - \beta(\omega_0) - \beta_1(\omega_0)[\omega - \omega_0]\} - \alpha(\omega)/2.$$

In these equations, $n_{eff}(\omega)$ and $A_{eff}(\omega)$ are the frequency-dependent effective refractive index and mode area, respectively; $\beta(\omega_0)$ and $\beta_1(\omega_0)$ are the propagation constant and its derivative at the centre frequency of pump pulses; $\alpha(\omega)$ is the loss; n_0 and n_2 are the linear and nonlinear refractive indices, respectively; c is the speed of light; $\Im$ and $\Im^{-1}$ denote the forward and inverse Fourier transformations, respectively; and $R(t)$ is the nonlinear response function of atmospheric air, which has the form $R(t) = (1 - f_R)\delta(t) + f_R h_R(t)$. Here, the former term, with the delta function, represents the Kerr effect and the latter term represents the contribution of the Raman scattering response, which relaxes more slowly. The Raman response function has the form [22]

$$h_R(t) = \Omega^2 \tau_s \exp\left(-\frac{t}{\tau_{dip}}\right)\sin\frac{t}{\tau_s},$$

where $\Omega^2 = \tau_s^{-2} + \tau_{dip}^{-2}$; $\tau_s = 1/\omega_R$; ω_R is the frequency of the transition between the J = 8 and 6 rotational levels of the

nitrogen molecule; $\tau_{dip} = 1/\Gamma_2$; and Γ_2 is the dephasing rate of the dipole moment of the J = 8 excited rotational state. In our calculations for ~100-fs pulses, we used $f_R = 0.5$, $\omega_R = 1.6 \times 10^{13}$ s^{-1} and $\Gamma_2 = 1.3 \times 10^{13}$ s^{-1} [23, 24].

Numerical analysis was carried out in the Matlab environment using built-in algorithms for performing the fast Fourier transform and solving the equation by the fourth-order Runge–Kutta method. In the case of femtosecond pulses, the guidance characteristics of fibre may strongly depend on wavelength, so in numerical analysis we took into account the spectral dependences of the effective mode area $A_{eff}(\omega)$, waveguiding loss $\alpha(\omega)$ and effective refractive index $n_{eff}(\omega)$. The guidance and dispersion characteristics of the fibre were calculated by the finite element method in the Femlab environment.

3. Optical fibre

The inset in Fig. 1 shows the cross section of the HCRF fabricated in this study, which has a transmission band in the 1.56-μm range. The fibre has eight capillaries with a wall thickness of 2.5 μm, a core diameter of 55 μm and an outer diameter of 140 μm. Figure 1 shows spectral dependences of quadratic dispersion and losses obtained with the parameters corresponding to the third transmission band of the hollow-core fibre in the wavelength range 1.45–1.7 μm in the ARROW model [27]. At a wavelength of 1.56 μm, the dispersion of the fibre is $\beta_2 = -1.42$ ps^2 km^{-1} (D = 1.1 ps nm^{-1} km^{-1}). The dispersion broadening length for Gaussian pulses of duration $\tau = 100$ fs is $L_d = t_0^2/\beta_2 = 2.54$ m. The loss at this wavelength is 0.175 dB m^{-1}. The effective absorption length, over which pulse propagation with a power loss within the e^{-1} level is possible, is $L_{eff} = 1/\alpha \approx$ 25 m. The calculated fundamental mode field diameter at a wavelength of 1.56 μm was determined to be 40 μm. The nonlinearity coefficient is $\gamma = 2\pi n_2/(\lambda A_{eff}) = 9.65 \times 10^{-8}$ m^{-1} W^{-1}, $n_2 = n_{2K} = 3 \times 10^{-23}$ m^2 W^{-1} and $A_{eff} = 1252$ μm^2. The nonlinear effects related to Kerr nonlinearity become significant at pulse powers $P > 400$ kW, where the nonlinear length $L_{nl} = 1/(\gamma P)$ is smaller than the effective absorption length L_{eff}.

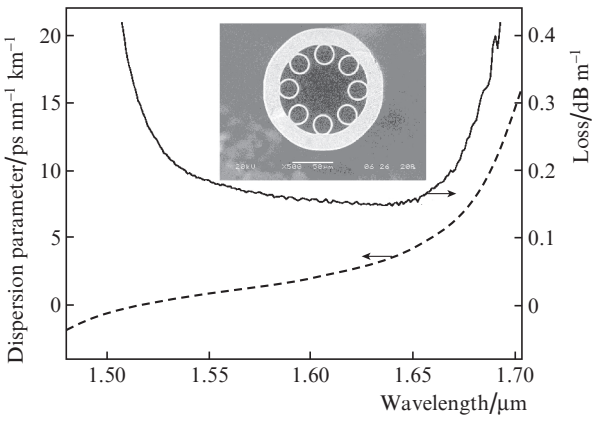

Figure 1. Spectral dependences of the dispersion parameter and optical loss for the HCRF fabricated in this study. Inset: cross section of the fibre.

4. Numerical analysis results and discussion

Figure 2 illustrates the propagation of a Gaussian pulse of ~100-fs duration through a fibre with an absorption length of 25 m at a pulse power of 3 kW. At this power, the nonlinear length $L_{nl} = 1/(\gamma P)$ considerably exceeds the dispersion length L_d and absorption length L_{eff}, so nonlinear effects do not manifest themselves and the pulse is influenced primarily by dispersion and losses. In particular, its spectral width is seen to remain unchanged (Fig. 2d), whereas its duration increases by a factor of 9.4 because of the dispersion (Fig. 2c). The output pulse power, which is determined by a combined effect of dispersion and losses, decreases by 25 times (Fig. 2b). The stronger pulse broadening at the trailing edge is due to the lower propagation velocity of the longer wavelength components in the negative dispersion region (the zero-dispersion wavelength in the transmission band under consideration is $\lambda_0 = 1.514$ μm). Such behaviour is observed up to pulse powers two orders of magnitude above 3 kW.

At pulse powers above 300 kW, where $L_d < L_{nl} < L_{eff}$, the nonlinearity contribution becomes significant, showing up mainly as a gradual narrowing of the spectrum and a decrease in the degree of dispersion-induced broadening. The narrowing of the spectrum of the Gaussian pulse in the negative dispersion region at $L_d < L_{nl}$ is caused by the fact that the pulse phase is influenced differently by the dispersion, which has a parabolic phase profile (linear chirp) throughout the pulse, and the Kerr nonlinearity, which has a parabolic phase profile only in the central part of the pulse. At the pulse powers in question, there is only a slight modulation of the pulse spectrum and shape.

Figures 3 and 4 illustrate the propagation of pulses through the fibre at pulse powers such that $L_{nl} < L_d$. The data were obtained for a 10-MW pulse power (the Kerr nonlinear length is then a factor of 2.5 smaller than the dispersion length). The rainbow colour map demonstrates that the pulse spectrum is shifted by 54 nm to the Stokes region, where its structure is far less clearly pronounced than that in the anti-Stokes region, which has several well-defined bands. Figure 3b shows the shift of the spectrum as a function of fibre length. The rate of the shift is largest over the first four metres of the fibre, where the spectrum experiences the strongest broadening due to self-phase modulation. The process of power transfer to the Stokes region of the spectrum during pulse propagation through the fibre is illustrated in Fig. 4. It follows from Fig. 4b that, at a fibre length of 2.5 m, the asymmetrically broadened spectrum overlaps the transmission band of the fibre at a −40 dB level relative to the maximum. The pulse spectrum contains eight wavelengths corresponding to cascade anti-Stokes and five wavelengths corresponding to Stokes shifts (75 cm^{-1}) of a rotational SRS transition in nitrogen with respect to the peak power wavelength (λ_{max} = 1578 nm). It is seen that, in the short-wavelength part of the spectrum at the wavelengths corresponding to the anti-Stokes components, the spectrum has dips, whereas at the wavelengths of the Stokes components there are maxima. The strong asymmetry of the spectrum and pulse envelope is the result of the trailing edge self-steepening due to nonlinearity dispersion, which causes the spectral components near the pulse peak to have higher velocity in comparison with the longer wavelength components at the trailing edge. Because of the rapid shift of the maximum, the spectrum is poorly structured in the Stokes region, whereas the structuring of the

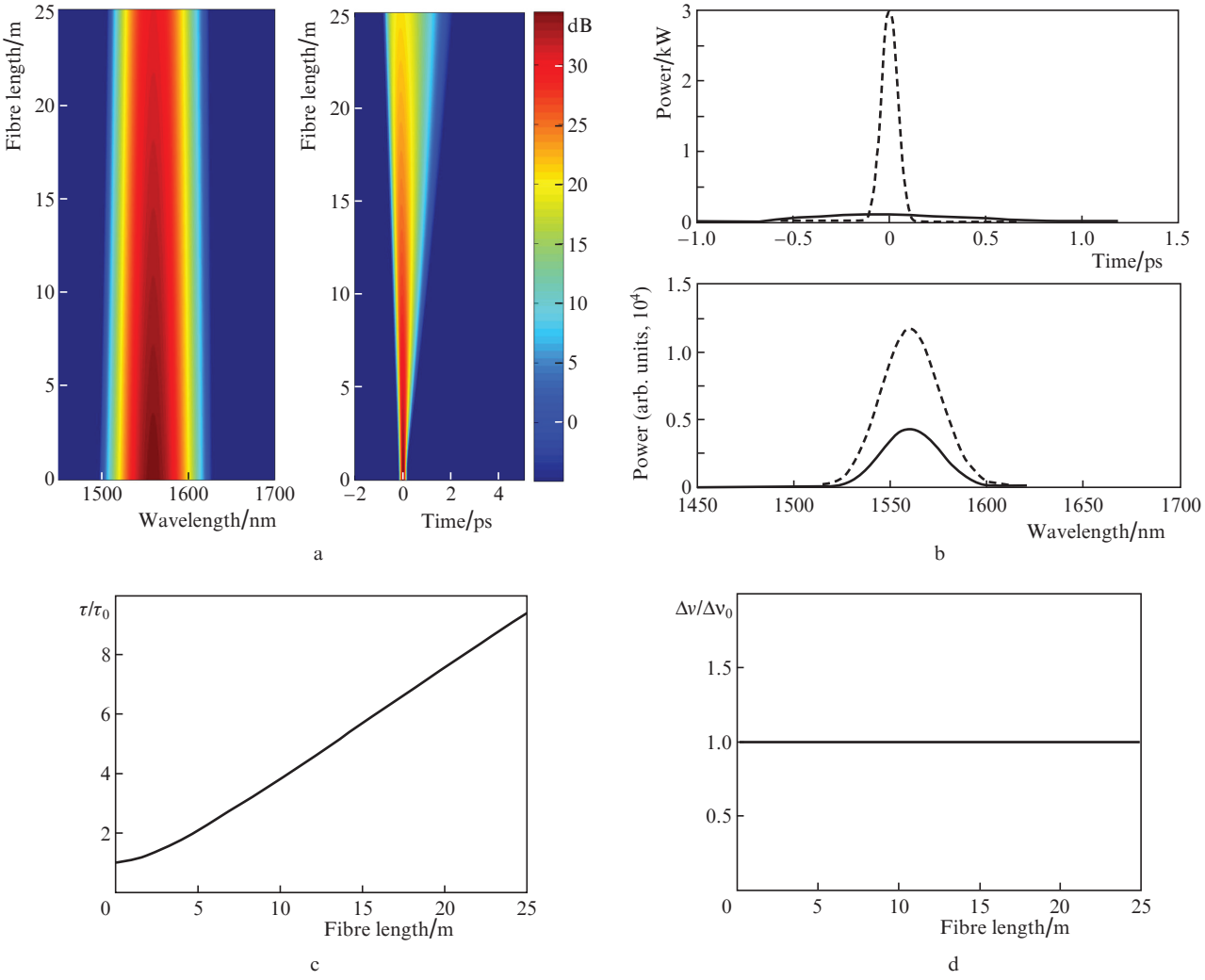

Figure 2. Propagation of a transform-limited Gaussian pulse of 100-fs duration through an HCRF (fibre length, 25 m; input pulse power, 3 kW): (a) rainbow colour maps illustrating the evolution of the pulse (in all the rainbow colour maps in this paper, the z axis is logarithmic with a dynamic range of 40 dB); (b) output pulse shape and spectrum (here and in Figs 4 and 5, dashed lines represent the input pulse); (c, d) ratios of the pulse duration and spectral width to their initial values for pulse propagation through the fibre.

spectrum in the anti-Stokes region becomes more pronounced as the pulse travels along the fibre (Figs 4d, 4f). Note that the power transfer to the Stokes region is accompanied by a considerable decrease in the power of the Stokes and anti-Stokes components in the pulse and a decrease in the rate of the shift of the spectral maximum. At a fibre length of 10 m, the spectrum shows three anti-Stokes and two Stokes components with respect to the maximum, which is shifted by 43 nm (λ_{max} = 1603 nm). The spectrum assumes a characteristic, asymmetric shape, with a fine structure in the short-wavelength region. The temporal pulse envelope has a broadened leading edge. During further propagation of the pulse through the fibre, the shape of its spectrum and its temporal envelope remain unchanged, its duration increases, and the width of its spectrum decreases.

As follows from Figs 3e and 3f, the time–bandwidth product of the pulse and the ratio of the pulse energy at half maximum to the total energy are constant (to within 1%) at fibre lengths from 8 to 25 m. This behaviour of the pulse allows it to be thought of as a Raman soliton, which retains its shape while propagating through the fibre. At the pulse power in question, the soliton order is N = 1.6. The rainbow colour maps in Fig. 3a and Figs 4d and 4f trace only the initial stage of the formation of a second soliton (at a –17 dB level) at a wavelength of 1546 nm.

Pulse decay into two Raman solitons is illustrated in Fig. 5, which shows rainbow colour maps for pulse evolution, temporal envelopes and the output spectrum of a 25-m length of the fibre at input pulse powers of 20 and 30 MW. In this case, phase modulation broadens the spectrum beyond the transmission band, and the shift of the spectrum of the first soliton with the highest energy reaches 100 (Fig. 5a) and 120 nm (Fig. 5c). The pulse loses energy, because the long-wavelength part of its spectrum extends beyond the band edge, and experiences a strong absorption.

Figure 6 shows different pulse parameters as functions of input pulse power at fibre lengths of 5, 12.5 and 25 m. It is seen in Fig. 6a that, at each of the fibre lengths under consideration, there exists a maximum output power, which decreases with increasing fibre length. At a fibre length of 5 m, the maximum output power P_{out} = 12.8 MW is reached at an input power P_{in} = 40 MW, with a transmission P_{out}/P_{in} = 0.31. At a fibre length of 12.5 m, the maximum value P_{out} = 5 MW is obtained at P_{in} = 25 MW and P_{out}/P_{in} = 0.2. At a

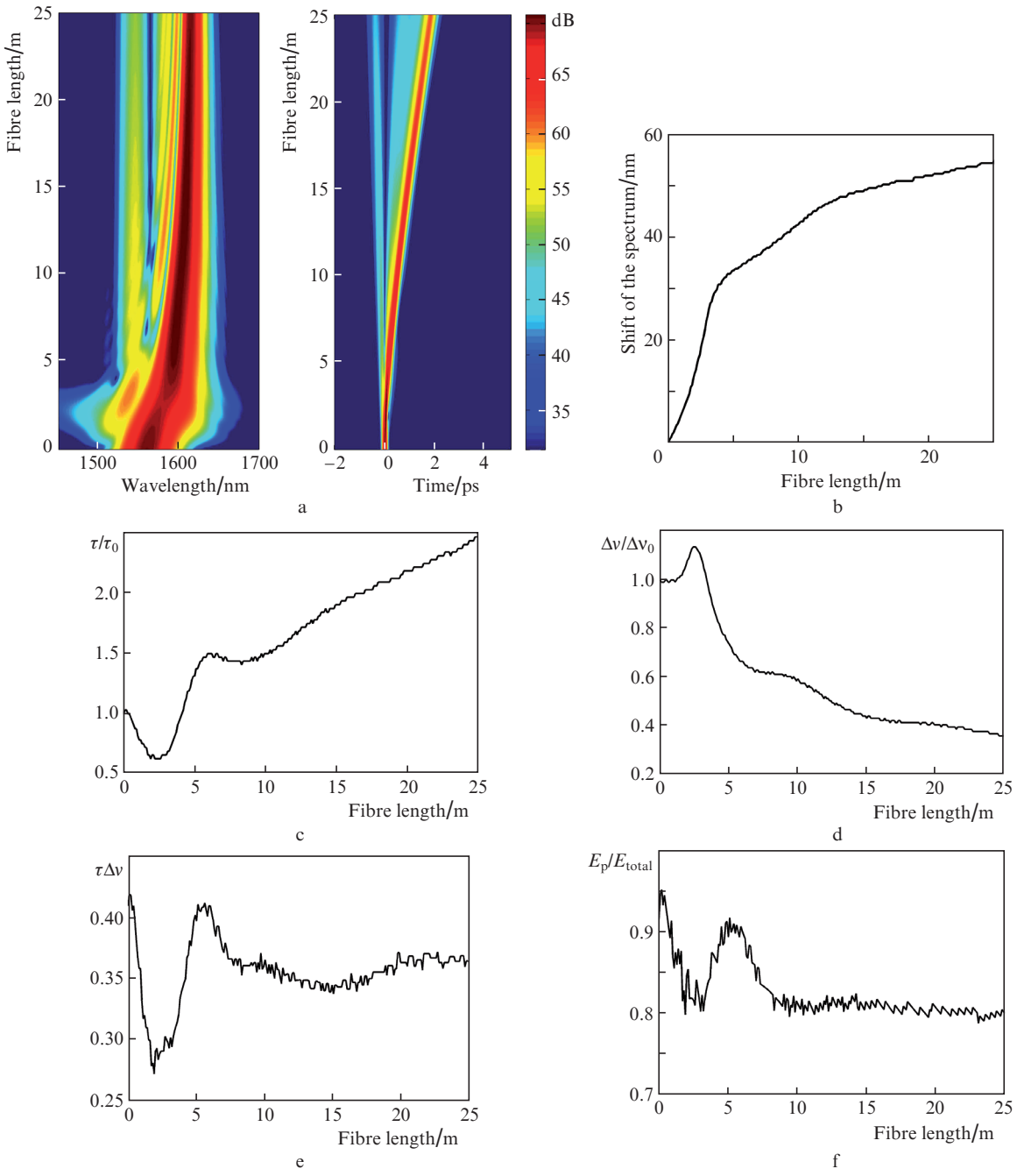

Figure 3. Propagation of a 100-fs transform-limited Gaussian pulse with an input power of 10 MW through an HCRF: (a) rainbow colour maps illustrating the evolution of the pulse; (b) shift of the spectrum; (c, d) duration and spectral width of the pulse propagating through the fibre; (e, f) time–bandwidth product and pulse energy as functions of fibre length.

fibre length of 25 m, the maximum value P_{out} = 1.9 MW is reached at P_{in} = 20 MW (P_{out}/P_{in} = 0.1).

The presence of maxima in $P_{out}(P_{in})$ follows from Fig. 6b, which shows how the emission wavelength varies with input pulse power. At a fibre length of 25 m, the maximum Stokes shift of 120–130 nm is reached at a power of 25–40 MW. At this shift, the maximum in the spectrum of a Raman soliton is located at the edge of the transmission band, where it experiences a strong absorption. At a fibre length of 5 m, the Stokes shift reaches the band edge at P_{in} = 50 MW.

Figure 6c shows the ratio of the pulse duration to its original value vs. input pulse power. The minimum broadening of the pulse, 1.2, 1.7 and 2.4 at fibre lengths of 5, 12.5 and 25 m, respectively, is observed at powers P_{in} = 8–15 MW. This power range corresponds as well to the maximum optical power transfer efficiency (P_{out}/P_{in} = 0.65, 0.31 and 0.14 at the above fibre lengths). At these input pulse powers, the broadening of the spectrum due to self-phase modulation and the Stokes shift have optimal values with respect to the transmission bandwidth (Fig. 3).

Figure 6d demonstrates that, at input powers from 8 to 50 MW, the time–bandwidth product $\tau\Delta\nu$ of the pulse, which characterises the pulse quality, ranges from 0.29 to 0.37. Therefore, the envelope of a Gaussian pulse propagating through the fibre becomes nearly sech-shaped ($\tau\Delta\nu$ = 0.32).

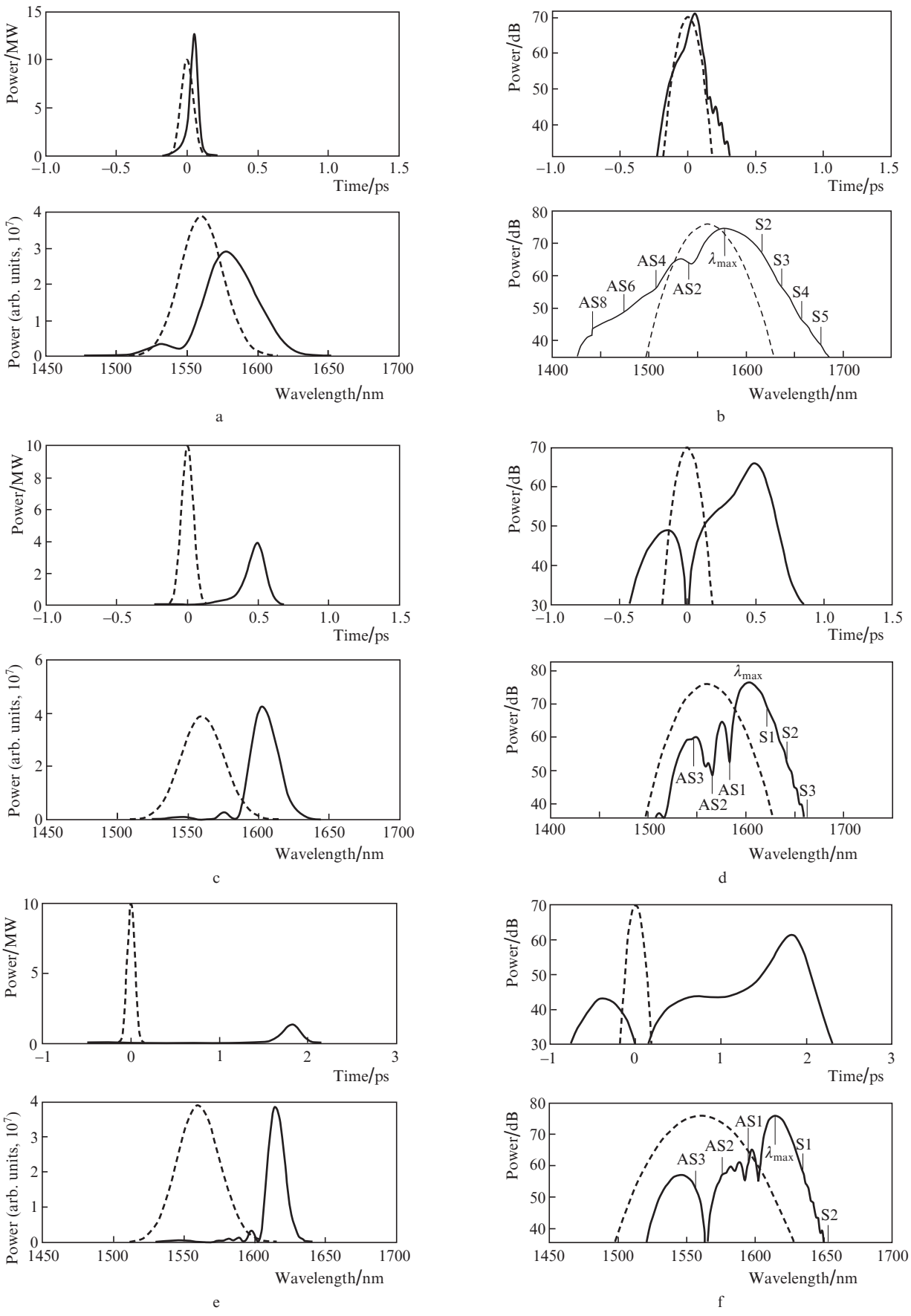

Figure 4. Evolution of the shape of the pulse spectrum at an input pulse power of 10 MW and fibre lengths of (a, b) 2.5, (c, d) 10 and (e, f) 25 m; (a, c, e) linear and (b, d, f) logarithmic vertical axes. S and AS are cascade Stokes and anti-Stokes components of a rotational SRS transition in nitrogen with respect to the pulse peak.

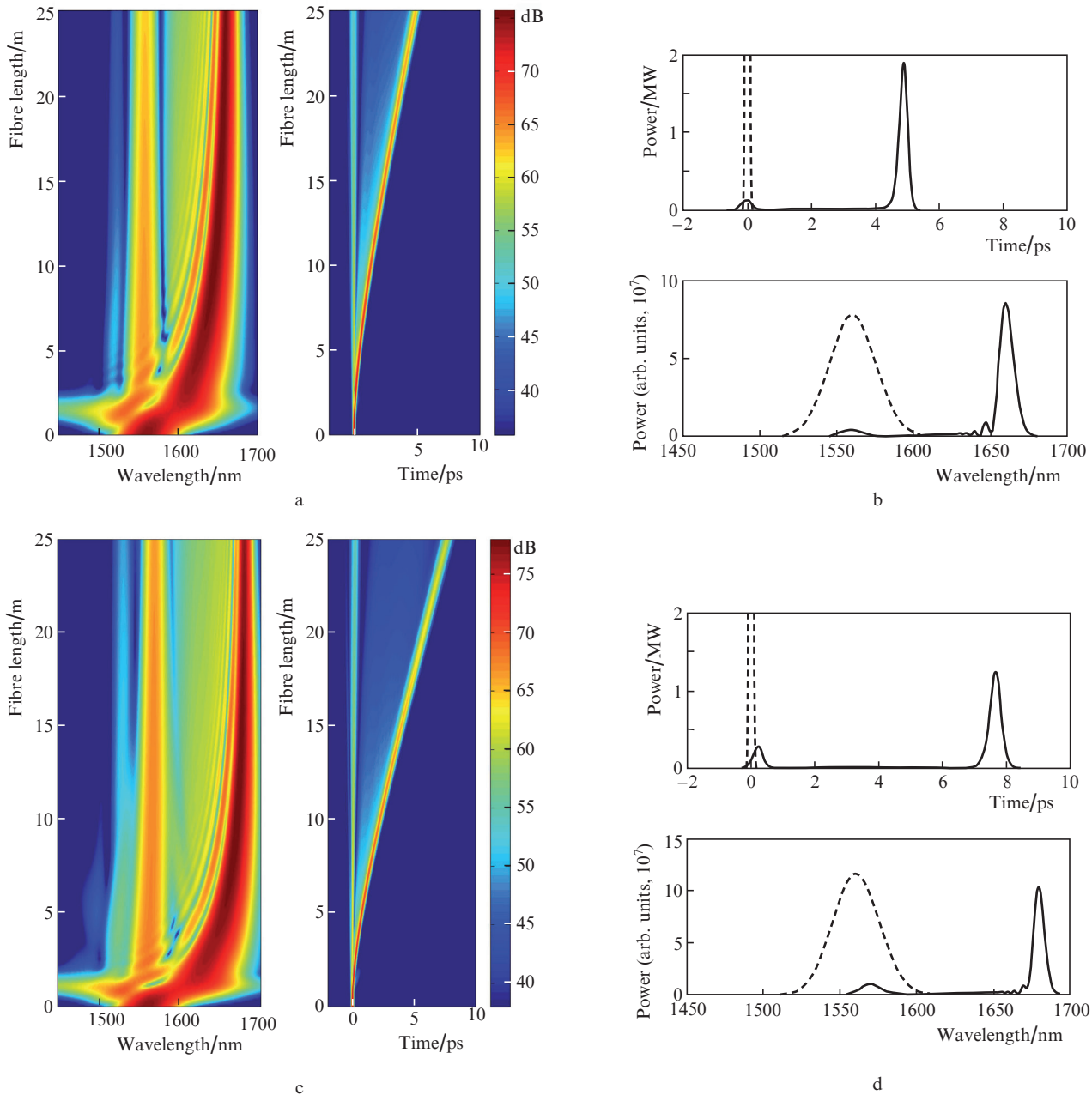

Figure 5. Formation of two Raman solitons over a length of 25 m during the propagation of a 100-fs transform-limited Gaussian pulse through an HCRF at pulse powers of (a, b) 20 and (c, d) 30 MW.

5. Experimental data on femtosecond pulse transmission in the linear propagation regime

To study the propagation of light in the HCRF, we used an erbium fibre laser generating 133.6-fs pulses of 0.14-nJ energy at a wavelength of 1.56 μm [28]. The laser output was coupled into the fibre (Fig. 1) up to 5 m in length with a coupling efficiency of 85%. Figure 7 shows spectra and autocorrelation traces of pulses at the fibre output. The pulse spectrum at the fibre input had a rather complex, parabolic shape, which remained unchanged at the output (Fig. 7a). The pulse duration measured after the pulse passed 2- and 5-m lengths of the fibre was 137 and 160 fs, respectively. The inset in Fig. 7b illustrates the evolution of the pulse duration, fitted by the function $\tau = \tau_0\sqrt{1 + (L/L_d)^2}$, which corresponds to pulses with a Gaussian-shaped envelope without frequency modulation, with a characteristic dispersion length $L_d = 7.5 \pm 0.2$ m. The characteristic dispersion length L_d thus obtained allows us to estimate the effective dispersion of the fibre at a wavelength of 1560 nm: $|\beta_2| = 8.6 \times 10^{-4}$ ps^2 m^{-1} ($|D| = 0.67$ ps nm^{-1} km^{-1}). Taking into account the complex shape of the spectrum and possible variations in dispersion along the length of the fibre due to the nonuniformity of its outer diameter, we conclude that the effective dispersion obtained agrees well with the value calculated by the finite element method from the fibre cross section (Fig. 1). The experimental data on femtosecond pulse transmission through the HCRF are well consis-

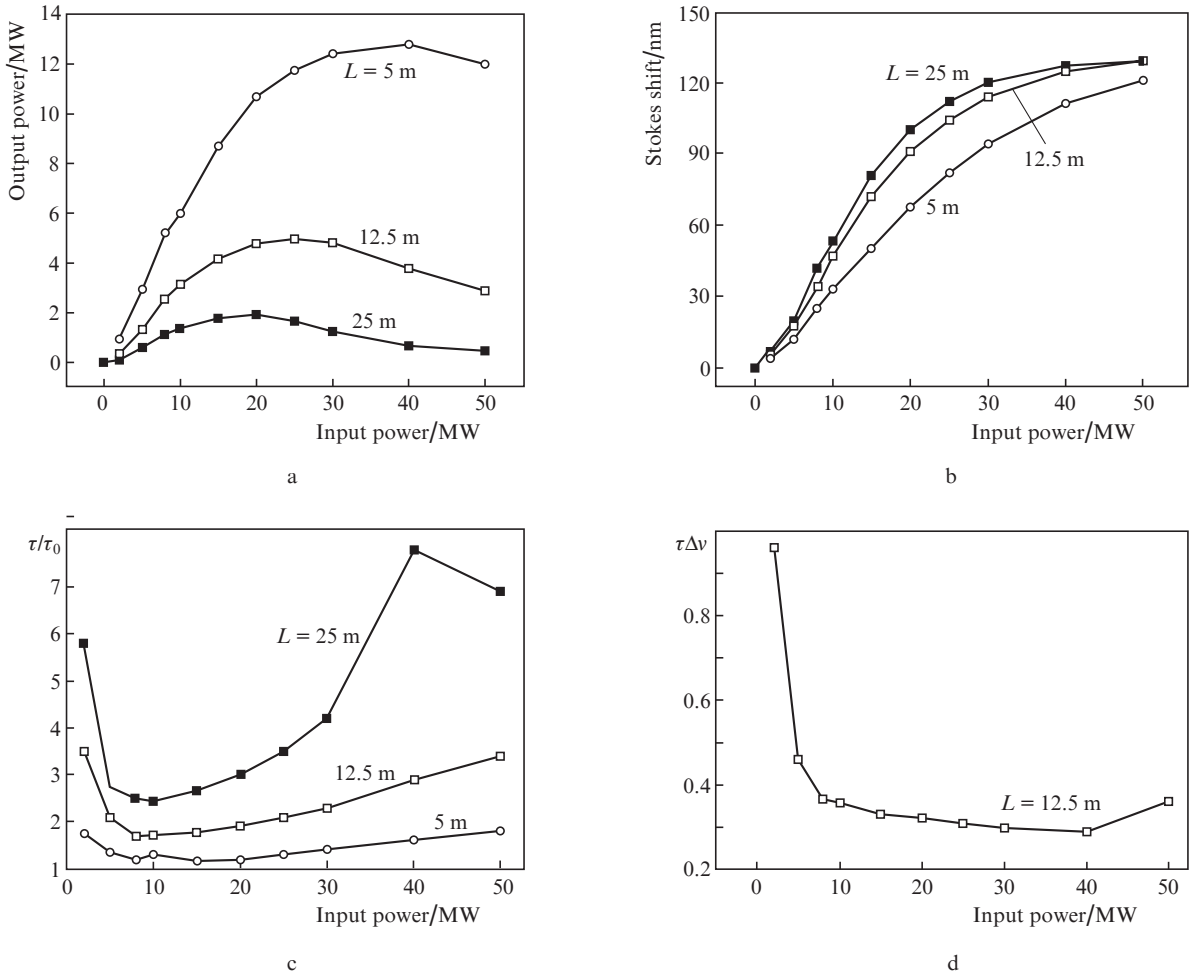

Figure 6. (a) Output pulse power, (b) shift of the spectrum, (c) pulse duration and (d) time–bandwidth product as functions of input pulse power at different fibre lengths L.

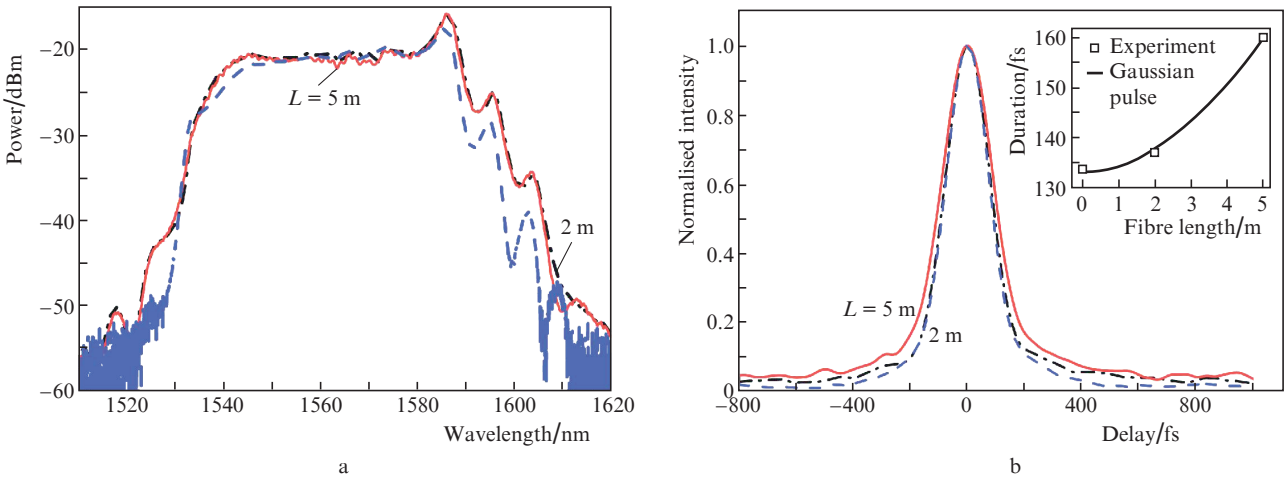

Figure 7. (a) Spectra and (b) autocorrelation traces of pulses with a Gaussian-shaped envelope at the output of 2- and 5-m-long hollow-core fibres (the dashed lines refer to the input pulse). Inset: femtosecond pulse duration as a function of fibre length.

tent with the numerical analysis results presented in Fig. 2 for kilowatt powers. In the case of the erbium fibre laser pulse power used in our experiments (P = 1 kW), nonlinear effects can be neglected (L_{nl} = 5.2 km) and a major role in pulse propagation is played by waveguide dispersion, which increases the pulse width by 20% for 5 m of the fibre.

6. Conclusions

We have fabricated a microstructured fibre with an air-filled hollow core and a cladding formed by one ring of cylindrical capillaries. The fibre has a transmission bandwidth of 250 nm in the 1.55-μm telecom range. It has a very low negative dispersion at a wavelength of 1.56 μm, low losses and a zero-dispersion wavelength shifted towards the short-wavelength edge of its transmission band. Numerical analysis of the propagation of 100-fs pulses of various powers through this hollow-core fibre has allowed two propagation modes to be distinguished, linear and nonlinear, which differ in power characteristics and potential practical applications.

The linear regime is limited by pulse powers of ~300 kW, at which $L_{nl} > L_{eff}$ and distortions of the pulse shape are caused primarily by waveguide dispersion. It has been shown theoretically and experimentally that the dispersion length in the fibre allows ~100-fs transform-limited pulses to be transmitted without distortions of their spectrum and with minimum changes in their duration over fibre lengths of the order of several metres. In this power range, the fibre is potentially attractive for use in information technologies and medical applications.

In the nonlinear regime ($L_{nl} < L_{eff}$), the HCRF studied here allows a 160-fs pulse more than 12 MW in power (pulse energy of 1.92 μJ) to be obtained at the output of a 5-m length of the fibre when a 100-fs pulse of 40-MW power (pulse energy of 4 μJ) is launched into the fibre. The highest power transfer efficiency (65% at a fibre length of 5 m) was reached at input powers in the range 10–15 MW, at which the broadening of the spectrum due to self-phase modulation and the Stokes shift have optimal values with respect to the transmission bandwidth. Radiation transmission in the form of megawatt Raman solitons, without broadening into a supercontinuum, is possible over the entire effective absorption length of 25 m. To the best of our knowledge, these power characteristics exceed those reported to date for ~100-fs pulses in other types of hollow fibres filled with atmospheric air.

Numerical analysis results demonstrate that pulse propagation in the hollow-core fibre differs significantly from that in a usual silica fibre, where soliton pulse propagation, without broadening into a supercontinuum, is possible at powers many orders of magnitude lower than those considered in this study. At low losses in a wide spectral range, characteristic of standard silica fibres, higher order dispersion terms lead to the generation and amplification of dispersion waves in the positive dispersion region, provided the phase matching condition is met. Along with higher order nonlinearities, this process leads to instability of a multisoliton pulse, transforming its spectrum into a supercontinuum. The HCRF fabricated in this study has a relatively narrow transmission window, in the range 1450–1700 nm, with a zero-dispersion wavelength (1514 nm) shifted towards the short-wavelength edge of its transmission band. In the case of a pulse at a wavelength of 1560 nm, phase matching, which ensures efficient soliton energy transfer to dispersion waves, is possible at wavelengths beyond the transmission band, so they cannot be amplified. The dominant process forming the structure of the spectrum is SRS, which ensures a power-dependent shift of the spectrum by up to 130 nm in this fibre.

It follows from numerical analysis results that the key factor limiting the power of ~100-fs megawatt pulses propagating through the fibre studied here is the Raman shift of their spectrum. Comparison of the present results with previous data obtained for Kagome lattice fibres by Wang et al. [9] and Debord et al. [10], who ensured transmission of two orders of magnitude more intense pulses of 600- to 800-s duration, leads us to conclude that the Raman shift, which varies inversely with pulse duration, can significantly limit the power of shorter pulses that can propagate through an air core.

The power characteristics obtained in the nonlinear propagation regime demonstrate that the HCRF fabricated in this study and filled with atmospheric air can be used for efficient transmission of high-power ~100-fs pulses in the 1.55-μm telecom range. Given its simple design, which requires neither filling of the fibre with gas under pressure nor vacuum pumping, the HCRF filled with atmospheric air is potentially attractive for materials processing applications. The fibre can also be used for tuning the emission wavelength of high-power femtosecond pulses over 130 nm in the 1.55-μm telecom range.

Acknowledgements. This work was supported by the Russian Foundation for Basic Research (Grant No. 14-29-07176 ofi_m).

References

1. Kosolapov A.F., Pryamikov A.D., Alagashev G.K., Kolyadin A.N., Biriukov A.S., Dianov E.M. *Specialty Optical Fibers (SOF). OSA Technical Digest (online)* (Barcelona, 2014) SoTu2B.3.
2. Travers J.C., Chang W., Nold J., Joly N.Y., Russell P.St.J. *J. Opt. Soc. Am. B*, **28**, A11 (2011).
3. Belli F., Abdolvand A., Chang W., Travers J.C., Russell P.St.J. *Optica*, **2**, 292 (2015).
4. Saleh M.F., Chang W., Holzer P., Nazarkin A., Travers J.C., Joly N.G., Russel P.St.J., Bioncalana F. *Phys. Rev. Lett.*, **107**, 203902 (2011).
5. Saleh M.F., Biancalana F. *Opt. Lett.*, **40**, 4218 (2015).
6. Ouzounov D., Ahmad F., Müller D., Venkataraman N., Gallagher M., Koch K., Gaeta A. *Science*, **301**, 1702 (2003).
7. Luan F., Knight J.C., Russell P.St.J., Campbell S., Xiao D., Reid D.T., Mangan B.J., Williams D.P., Roberts P.J. *Opt. Express*, **12**, 835 (2004).
8. Agrawal G.P. *Nonlinear Fiber Optics* (New York: Acad. Press, 2007).
9. Wang Y.Y., Peng X., Alharbi M., Dutin C.F., Bradley T.D., Gérôme F., Mielke M., Booth T., Benabid F. *Opt. Lett.*, **37**, 3111 (2012).
10. Debord B., Alharbi M., Vincetti L., Husakou A., Fourcade-Dutin C., Hoenninger C., Mottay E., Gérôme F., Benabid F. *Opt. Express*, **22**, 10735 (2014).
11. Pryamikov A.D., Biriukov A.S., Kosolapov A.F., Plotnichenko V.G., Semjonov S.L., Dianov E.M. *Opt. Express*, **19**, 1441 (2011).
12. Yu F., Wadsworth W.J., Knight J.C. *Opt. Express*, **20**, 11153 (2012).
13. Yu F., Knight J.C. *IEEE J. Sel. Top. Quantum Electron.*, **22**, 4400610 (2016).
14. Gladyshev A.V., Kolyadin A.N., Kosolapov A.F., Yatsenko Yu.P., Pryamikov A.D., Biryukov A.S., Bufetov I.A., Dianov E.M. *Kvantovaya Elektron.*, **45**, 807 (2015) [*Quantum Electron.*, **45**, 807 (2015)].
15. Alagashev G.K., Pryamikov A.D., Kosolapov A.F., Kolyadin A.N., Lukovkin A.Yu., Biriukov A.S. *Laser Phys.*, **25**, 055101 (2015).
16. Kolyadin A.N., Kosolapov A.F., Pryamikov A.D., Biriukov A.S., Plotnichenko V.G., Dianov E.M. *Opt. Express*, **21**, 9514 (2013).
17. Kolyadin A.N., Alagashev G.K., Pryamikov A.D., Mouradian L., Zeytunyan A., Toneyan H., Kosolapov A.F., Bufetov I.A. *Phys. Procedia*, **73**, 59 (2015).
18. Couairon A., Mysyrowicz A. *Phys. Proc.*, **441**, 47 (2007).
19. Shimoji Y., Fay A.T., Chang R.S.F., Djeu N. *Phys. Rep.*, **6**, 1994 (1989).

20. Skeldon M.D., Bahr R. *Opt. Lett*., **16**, 366 (1991).
21. Nibbering E.T.J., Grillon G., Franco M.A., Prade B.S., Mysyrowicz A. *J. Opt. Soc. Am. B*, **14**, 650 (1997).
22. Sprangle P., Penano J.R., Hafizi B. *Phys. Rev. E*, **66**, 046418 (2002).
23. Penano R., Sprangle P., Serafim P., Hafizi J.B., Tang A. *Phys. Rev. E*, **68**, 056502 (2003).
24. Penano J.R., Sprangle P., Hafizi B., Ting A., Gordon D.F., Kapetanakos C.A. *Phys. Plasmas*, **11**, 2865 (2004).
25. Loriot V., Hertz E., Faucher O., Lavorel B. *Opt. Express*, **17**, 13434 (2009).
26. Dudley J., Taylor R. *Supercontinuum Generation in Optical Fibers* (Cambridge: University Press, 2010).
27. Litchinitser N.M., Abeeluck A.K., Headley C., Eggleton B.J. *Opt. Lett*., **27**, 1592 (2002).
28. Krylov A.A., Sazonkin S.G., Lazarev V.A., Dvoretskiy D.A., Leonov S.O., Pnev A.B., Karasik V.E., Grebenyukov V.V., Pozharov A.S., Obraztsova E.D., Dianov E.M. *Laser Phys. Lett*., **12**, 065001 (2015).